HHS Public Access

Author manuscript

Science. Author manuscript; available in PMC 2020 June 21.

Published in final edited form as:

Science. 2019 June 21; 364(6446): 1170–1174. doi:10.1126/science.aav7019.

Direct arene C-H fluorination with $^{18}F^-$ via organic photoredox catalysis

Wei Chen[1,*], **Zeng Huang**[1,*], **Nicholas E. S. Tay**[2,*], **Benjamin Giglio**[1], **Mengzhe Wang**[1], **Hui Wang**[1], **Zhanhong Wu**[1], **David A. Nicewicz**[2,†], **Zibo Li**[1,†]

[1]Biomedical Research Imaging Center, Department of Radiology, and UNC Lineberger Comprehensive Cancer Center, University of North Carolina–Chapel Hill, Chapel Hill, NC 27514, USA.

[2]Department of Chemistry, University of North Carolina–Chapel Hill, Chapel Hill, NC 27599, USA.

Abstract

Positron emission tomography (PET) plays key roles in drug discovery and development, as well as medical imaging. However, there is a dearth of efficient and simple radiolabeling methods for aromatic C–H bonds, which limits advancements in PET radiotracer development. Here, we disclose a mild method for the fluorine-18 (^{18}F)–fluorination of aromatic C–H bonds by an [^{18}F]F^- salt via organic photoredox catalysis under blue light illumination. This strategy was applied to the synthesis of a wide range of ^{18}F-labeled arenes and heteroaromatics, including pharmaceutical compounds. These products can serve as diagnostic agents or provide key information about the in vivo fate of the labeled substrates, as showcased in preliminary tracer studies in mice.

Fluorine-18 (^{18}F) is one of the most important radioisotopes in the radiopharmaceutical industry because it has a relatively long half-life ($t_{1/2}$ = 110 min) and decays with high efficiency by positron emission (97%) (1). A primary application of this radioisotope is in the form of 2-[^{18}F]fluorodeoxyglucose ([^{18}F]FDG), which is used for oncological

†Corresponding author. nicewicz@unc.edu (D.A.N.); ziboli@med.unc.edu (Z.L.).
*These authors contributed equally to this work.

Author contributions: W.C. established the final labeling conditions and conducted the majority of the aromatic labeling experiments. Z.H. established the initial labeling conditions and ran a portion of the aromatic labeling scope. N.E.S.T. identified the ^{19}F-fluorination conditions and the catalyst system, synthesized ^{19}F-aromatic standards, and co-wrote the manuscript. B.G. contributed to the initial labeling design and discussion. M.W. performed initial labeling and PET imaging experiments. H.W. established the inflammation and tumor models and performed PET imaging analysis. Z.W. contributed to the initial labeling design and discussion. D.A.N. and Z.L. conceived and supervised the project and experiments and also co-wrote the manuscript.

Competing interests: N.E.S.T. and D.A.N. are inventors on a patent filed by UNC currently pending (U.S. Patent Application No. 15/826,092).

Data and materials availability: Experimental procedures, additional data, and analysis are included in the supplementary materials. Data for PET and PET/CT images in Fig. 3 and figs. S94 and S95 have been submitted to Zenodo (43–47).

SUPPLEMENTARY MATERIALS
science.sciencemag.org/content/364/6446/1170/suppl/DC1
Materials and Methods
Figs. S1 to S101
Tables S1 to S58
Spectral Data
Radio-HPLC Traces
References (48–81)
Movies S1 to S3

diagnoses, neuroimaging, and studying glucose metabolism (2). Uptake of [^{18}F]FDG and other ^{18}F-labeled agents is monitored by positron emission tomography (PET) imaging, which quantifies spatial distributions and metabolic perturbations, as well as site-specific chemical reactivity and ensuing in vivo biological processes (3).

Many small-molecule pharmaceuticals and therapeutics contain aromatic or heteroaromatic systems within their framework, thus presenting a common organic subunit for the installation of radioisotopes to yield radiotracers with imaging utility. In particular, the direct conversion of arene C–H into C–^{18}F bonds is ideal owing to the prevalence of aromatic C–H bonds and the increasing importance of C(sp^2)–F bonds in small-molecule therapeutics and probes (4, 5). Direct ^{18}F-fluorination of aromatics currently requires the use of electrophilic fluorine sources, the simplest of which is [^{18}F]F_2; however, this gaseous reagent is incompatible with many common organic functional groups and suffers from low molar activity (the measured radioactivity per mole of compound) as a result of its production methods (6–8). Most modern methods for C–H to C–F bond conversion require electrophilic fluorine in the form of relatively expensive but bench-stable reagents such as N-fluorobenzenesulfonimide (NFSI) and 1-chloromethyl-4-fluoro-1,4-diazoniabicyclo[2.2.2]octane-bis(tetra-fluoroborate) (Selectfluor). However, their utility for ^{18}F radio-labeling via electrophilic fluorination is diminished because [^{18}F]NFSI and [^{18}F]Selectfluor are prepared from [^{18}F]F_2 (9), which results in even lower molar activities of the ^{18}F-labeled tracers. Therefore, a method for direct conversion of a C–H to a C–^{18}F bond via a nucleophilic arene fluorination strategy is highly attractive because the synthesis of ^{18}F-radiolabeled pharmaceutical compounds can be accomplished with high molar activity fluoride ([^{18}F]F^-). Furthermore, direct C–H to C–^{18}F conversion should alleviate synthetic burdens associated with the synthesis of radiotracer precursors (10) and allow for the recovery of precious, unreacted starting material. However, the primary hurdle for this approach is the lack of reactivity for a majority of simple aromatics with [^{18}F]F^-.

Nucleophilic aromatic substitution of electron-deficient arenes has been the standard method for [^{18}F]F^- incorporation (1), but prefunctionalization of the aromatic subunit with electron-withdrawing groups is required for this strategy (3). Thus, modern radiofluorination methods have sought to generalize the arene scope for this transformation. Current strategies include ^{18}F-deoxyfluorination of phenols via uronium (11) and N-arylsydnone (12) intermediates; displacement of sulfonium salts (13); fluorodemetalation of preformed palladium or nickel arene complexes from the requisite aryl halides or boronic acids (14, 15); and copper-mediated cross-coupling of preformed or in situ–generated aryliodoniums (16, 17), aryl boronic acids (18), esters (19), and arylstannanes (20) (Fig. 1A). Despite the advances in radiofluorination, these approaches can be technically challenging for radiochemists. Moreover, the use of metal re-agents, especially in stoichiometric or super-stoichiometric amounts, can complicate the quality control process for translational studies because additional analysis on residual metal levels is required.

With these challenges in mind, we sought to develop an arene C–H fluorination method compatible with [^{18}F]F^- (Fig. 1B). The Nicewicz lab has developed a research program using organic single-electron photooxidants to catalytically generate arene radical cations as reactive intermediates for arene C–H functionalization reactions. Thus, we applied this

strategy for direct C–H to C–^{18}F bond conversion. Considering the low molar amount of no-carrier-added [^{18}F]F^{-}, radiation exposure, and the potentially high cost of [^{18}F]F^{-} production, we decided to first use ^{19}F-fluoride for the development of a photoredoxcatalyzed method for arene C–H fluorination. Using diphenyl ether as the aromatic substrate, we were able to obtain *17*% of fluorinated adducts in a 13:1 para:ortho ratio using an acridinium-based photooxidant (**1**), cesium fluoride (CsF), the phase-transfer reagent tetrabutylammonium bisulfate (TBA-HSO_4) and 2,2,6,6-tetramethyl-1-piperidine 1-oxyl (TEMPO) as a redox co-mediator under aerobic conditions for *24* hours (Fig. 2 and table S1). We attribute the low yields to the relative recalcitrance of fluoride, which is a Brønsted base and can form strong hydrogen bonds in aqueous environments (21). Despite lower yields for the aryl C–H fluorination with ^{19}F^{-}, C–H fluorination was feasible and thus we decided to extend our method to radiofluorination.

In this new system, [^{18}F]F^{-} is employed as the limiting reagent, and we envisioned that the relatively higher concentration of arene radical cation would efficiently capture [^{18}F]F^{-}. Transitioning from F^{-} to [^{18}F]F^{-} necessitated a reexamination of fluoride sources and irradiation method while aiming to achieve reasonable ^{18}F-labeling yields on 30 min to 1 hour time scales, given the fleeting half-life of the fluorine radio-isotope. High molar activity aqueous [^{18}F]F^{-} is prepared via proton bombardment of [^{18}O] water and subsequent elution of ^{18}F-fluoride with tetrabutylammonium bicarbonate to yield [^{18}F]TBAF, or potassium carbonate complexed with the aminopolyether cryptand Kryptofix 2.2.2 to form [^{18}F]KF-K_{222} (1). In both of these systems, excess tetrabutylammonium bicarbonate and potassium carbonate are present. Although the initial radio-chemical yields (RCYs) were relatively low (0.57%), [^{18}F]TBAF was the most effective ^{18}F-fluorinating agent in the synthesis of [^{18}F]**2** [see section 5.5 of the supplementary materials and methods (SM 5.5)]. Initial RCYs using *455*-nm light-emitting diodes were relatively low (*0.57%*), which prompted us to reevaluate the light flux for the transformation. Using top-down irradiation with a *3.5*-W laser (*450* nm) (22) for *30* min (cooled to 0°C to prevent solvent loss from laser-generated heat) under an aerobic atmosphere afforded a marked increase in the yields of the ^{18}F-fluorinated adducts of diphenyl ether (*25.8* and *2.0*% for the para and ortho adducts, respectively). After extensive optimization (SM 5.5), we identified a system that afforded the para and ortho fluorinated adducts (*37.1* and *2.0*% yield, respectively) but observed a drop in the molar activity of [^{18}F]-TBAF. We attributed this inconsistency to the exchange of [^{18}F]F^{-} with fluoride from the BF_4^{-} counterion of the acridinium catalyst, which in turn lowers the net molar activity of [^{18}F]-TBAF. To circumvent this problem, we synthesized an acridinium containing a perchlorate (ClO_4^{-}) counterion and found that ^{18}F-labeled diphenyl ether (**2**) adducts could be isolated with a molar activity of 1.37 Ci/μmol (compared with 0.39 Ci/μmol with BF_4^{-} counterion) and comparable RCYs of 38.2 and 1.8% for the para and ortho products, respectively.

Having identified the optimal catalytic conditions for the transformation, we turned our attention to evaluating the scope of this method with a range of aromatic and heteroaromatic substrates. Biphenyl (**3**) and naphthalene (**4**) were fluorinated at the 4- and 1-positions, respectively, in good RCY. 2-Substituted methoxyarenes (**5** to **11**) were also efficiently fluorinated at the C–H site para to the methoxy group, following a similar trend to the

amination (23) and cyanation (24) methods from our laboratory. Halogenated and pseudohalogenated methoxyarenes 2-bromoanisole (**5**), 2-chloroanisole (**6**), and 2-OTf-anisole (**7**) were all fluorinated at the 4-position in good RCY, thus demonstrating the compatibility of halogenated and pseudohalogenated arenes with our system, as these functional groups are typically susceptible to oxidative addition in transition metal–catalyzed methods. A range of carbonyl-containing functional groups, such as esters (**8**), ketones (**9**), nitriles (**10**), aldehydes (**11**), and amides (**12**), were all compatible with this method, affording single regioisomers of the ^{18}F adducts. Methoxy-substituted biphenyl systems (**13** and **14**) were also competent substrates for fluorination, affording the single regioisomers in moderate RCY. We did not observe significant ortho fluorination for 2-substituted anisoles, which we attribute to a greater gain in positive charge density on the para position of the arene cation radical (25) and potential steric hindrance. Thus, we were curious to explore the amenability of our radiofluorination protocol to methoxyarenes bearing substitution at the para position. We found that these 4-substituted congeners (**15** to **19**) were compatible fluorination partners, although the RCYs observed were significantly lower than their 2-substituted counterparts. Nevertheless, the isolated yields for these 4-substituted methoxyarenes are acceptable for PET imaging applications. Preliminary computational studies (figs. S97 and S98) suggest that there is little correlation between the calculated electrophilicities of the cation radical for the 2- and 4-substituted arenes and the observed yields, thus suggesting a greater contribution of steric effects in determining site selectivity. When 3-methoxyacetophenone was subjected to the radiofluorination conditions, a 2:1 ratio of ^{18}F-labeled adducts was obtained with a preference for fluorination para to the methoxy group (20). Computational studies suggest that the 6-position gains the most electrophilic character relative to the 2- and 4-positions (fig. S99) upon single electron oxidation; however, only the latter products are observed. Taken together, these results demonstrate a strong preference for the para functionalization of methoxyarenes except in cases where the para position is occupied, and they suggest that steric effects may play a role in dictating site selectivity for C–H fluorination.

Arenes containing guaiacol motifs are found in numerous plant and animal metabolites; thus, the application of our C–H radiofluorination strategy could enable the facile synthesis of ^{18}F radio-tracers from renewable sources. We found that ethylguaiacol (**21**), vanillylamine (**22**), nonivamide (**23**), and zingerone (**24**) derivatives were all successfully fluorinated to provide single regioisomers of the ^{18}F analogs. Furthermore, this reaction is not limited to methoxyarenes, as demonstrated by mesitylene undergoing fluorination (<9%) under aerobic conditions to give *25*. This isolated RCY was improved to 50% by employing a modified anaerobic system (using TEMPO as a net oxidant in MeCN with N_2 bubbling). Fluorinated heterocycles are privileged and highly desirable motifs in pharmaceutical and agro-chemical research, and substantial resources are directed toward measuring the pharmacokinetics of these compounds (26). Our radiofluorination protocol was applied to several heterocyclic classes: We found that *2,5*-dimethoxypyridine (**26**), 2-chloro-6-methoxyquinoline (**27**), and N,N-dihexylquinazolinedione (**28**) were all successfully fluorinated in good to moderate RCY. Benzazoles common to many therapeutics, such as N-methylindazole (**29**), benzoxazole (**30**), and benzimidazole (**31**), all underwent fluorination at the most electrophilic positions of their respective cation radicals. Selective late-stage arene C–H

fluorination is an attractive synthetic strategy, as it circumvents the need for complicated labeling precursors and enables the straightforward conversion of bioactive molecules and drugs into PET agents for in vitro companion diagnosis or for pharmacodynamic and pharmacokinetic studies.

We chose to apply our ^{18}F radiofluorination method to several nonsteroidal anti-inflammatory drugs (NSAIDs), which are an important class of pharmaceuticals that alleviate pain and inflammation by inhibiting the activity of cyclooxygenase enzymes (COX-1 and COX-2). Although there have been recent advances in the radiolabeling of COX-1 and COX-2 inhibitors, many examples use ^{11}C as the radionuclide, which has the disadvantage of a shorter half-life ($t_{1/2}$ = *20.2* min) than ^{18}F (27). Existing ^{18}F-labeled COX inhibitors typically incorporate ^{18}F in the radioprobe as part of a phenol-appended fluorinated alkyl chain (28). However, these functional groups are prone to metabolic degradation and thus may be less-effective radiotracers (27, 29). Fluorination of the aromatic ring is a strategy typically used to study drug metabolism, as fluorine is a hydrogen bioisostere and its substitution slows the metabolic degradation of drug molecules by cytochrome P450 (29). Fluorinated aromatics can also act as metabolic tracers because hydroxylated fluoroarene metabolites undergo a 1,2-fluoride shift (NIH shift), thus allowing for the detection and quantification of metabolic byproducts (30, 31). Furthermore, the introduction of fluorine into the aromatic system can improve the potency and cell permeability of drug molecules through noncovalent interactions (5). The development of the NSAID celecoxib is an instructive example, in which the substitution of various aryl C–H bonds for aryl C–F bonds was used to bias in vitro COX-2 selectivity (32). However, routes for the analogous synthesis of C(sp^2)–^{18}F bonds in COX inhibitors with aromatic moieties are underexplored because of difficulties with designing late-stage precursors for ^{18}F radiolabeling (33). Thus, we envisioned that our method would enable the introduction of ^{18}F into known COX inhibitors. The NSAID derivatives fenoprofen methyl ester (**32**), flurbiprofen methyl ester (**33**), and *O*-methyl methyl salicy-late (**8**) were all fluorinated in good to moderate RCYs. Given the ubiquitous use of these commercial NSAIDs (34), the synthesis of their radio- tracer counterparts could provide researchers with a method for visualizing their immediate in vivo metabolic fates that is complementary to the longitudinal metabolism studies enabled by ^{3}H- and ^{14}C-labeling strategies (35).

The hypolipidemic agents clofibrate (**34**) and fenofibrate (**35**), as well as a derivative of the biological neurotransmitter precursor DL-DOPA (**36**), were selectively fluorinated in moderate RCY after *30* min. We found that the fluorination protocol was influenced by reaction times, as extending the runtime to 1 hour increased the RCY of the fluorinated DOPA derivative to 21.2%. This result is especially noteworthy because [^{18}F]DOPA is an important radioprobe for the PET imaging of CNS disorders (36), but published routes to it typically require extensive and sensitive synthesis with ^{18}F precursors (37) or the fluorination of prefunctionalized DOPA analogs (16, 19). This fluorinated DOPA derivative was then subjected to facile global deprotection to yield [^{18}F]-DOPA (**37**) in *12.3*% RCY. Other aromatic amino acids, such as the protected variants of O-Me-*ortho*-tyrosine and 4-phenyl-phenylalanine, were also successfully radiofluorinated (**38** and **40**, respectively), and their deprotected forms (**39** and **41**, respectively) were accessed with relative ease.

A major objective of our synthetic methodology was to develop clinically relevant PET tracers from readily available bioactive molecules without first requiring arene prefunctionalization. To test this concept, we examined the feasibility of converting the NSAID fenoprofen into a PET agent by direct C–H fluorination. Fenoprofen has notable anti-inflammatory activity (38), but there have been minimal studies with its fluorinated analogs. Given the widely exploited hydrogen bioisosterism of fluorine in medicinal chemistry (5), we were interested in examining the viability of the radiofluorinated analog for PET studies. [^{18}F]-Fenoprofen (**42**) was readily accessed from **32**, which was then used to detect inflammation induced by 12-*o*-tetradecanoylphorbol-13-acetate (TPA) in mouse ears (Fig. 3A and fig. S94) (see supplementary materials and methods for more details) (39). Preliminary ex vivo PET studies (Fig. 3A) show significantly higher up-take of [^{18}F]-fenoprofen in the ear inflammation model relative to the control 30 min after intravenous introduction of the radioprobe. These data suggest that **42** is a potential PET agent that demonstrates preferential accumulation in inflamed tissue. Additional biological evaluations for **42** are needed but are currently beyond the scope of this Report.

Another application of our C–H radiofluorination method is rapid radioligand screening in drug discovery and development. We chose to highlight synthetic aromatic amino acids as a class of bioactive metabolites owing to their applicability for oncological PET imaging (40–42). We are especially interested in the tyrosine scaffold, as fluorination on the aromatic ring is an important functionalization mode for developing PET probes. We selected O-Me-*ortho*-tyrosine and 4-phenyl-phenylalanine as the working examples, and our method provides facile access to radio-fluorinated **39** and **41**. In vivo PET studies of mice containing MCF7 (breast cancer) and U87MG (glioblastoma) tumor xenografts demonstrate prominent uptake of **39** with minimal accumulation in other organs except the pancreas and bladder (Fig. 3B and fig. S95) (see supplementary materials and methods for more details). Conversely, **41** displayed low uptake in similar tumor models with significantly higher retention in the mouse circulatory system. On the basis of these preliminary studies, **39** shows promise as a selective amino acid radioprobe for tumor detection, and further studies will be needed to examine its biological activity and pharmacology. These results further demonstrate the potential of our radiofluorination method for the discovery of new PET agents that circumvents the need for prefunctionalized (hetero)arenes.

^{18}F radiolabeling is an important tool for noninvasive studies of biological systems, and we anticipate that the applicability of our radio-fluorination method to commercial pharmaceuticals and metabolites will enable direct access to new classes of translationally relevant ^{18}F radio-tracers, either as diagnostic agents or as target probes for elucidating the in vivo fate of metabolites or pharmaceuticals.

Supplementary Material

Refer to Web version on PubMed Central for supplementary material.

ACKNOWLEDGMENTS

Funding: Financial support was provided in part by the National Institutes of Health (NIGMS) awards R01GM120186 (D.A.N.) and 5R01EB014354 (Z.L.) and by the UNC Department of Radiology, Biomedical

Research Imaging Center, and UNC Lineberger Comprehensive Cancer Center (start-up fund to Z.L.). N.E.S.T. is grateful for an NSF Graduate Research Fellowship. PET instrumentation was supported via an NIH High-End Instrumentation Grant (1S10OD023611–01).

REFERENCES AND NOTES

1. Preshlock S, Tredwell M, Gouverneur V, Chem. Rev 116, 719–766 (2016). [PubMed: 26751274]
2. Kelloff GJ et al., Clin. Cancer Res 11, 2785–2808 (2005). [PubMed: 15837727]
3. Coenen HH et al., Nucl. Med. Biol 37, 727–740 (2010). [PubMed: 20870148]
4. Gillis EP, Eastman KJ, Hill MD, Donnelly DJ,Meanwell NA, J. Med. Chem 58, 8315–8359 (2015). [PubMed: 26200936]
5. Meanwell NA, J. Med. Chem 61, 5822–5880 (2018). [PubMed: 29400967]
6. Nickles RJ, Daube ME, Ruth TJ, Int. J. Appl. Radiat. Isot 35, 117–122 (1984).
7. Krzyczmonik A, Keller T, Kirjavainen AK, Forsback S,Solin O, Labelled Comp J. Radiopharm. 60, 186–193 (2017).
8. Coenen HH et al., Nucl. Med. Biol 55, v–xi (2017). [PubMed: 29074076]
9. Teare H et al., Angew. Chem. Int. Ed 49, 6821–6824 (2010).
10. Taylor NJ et al., J. Am. Chem. Soc 139, 8267–8276 (2017). [PubMed: 28548849]
11. Neumann CN, Hooker JM, Ritter T, Nature 534, 369–373 (2016). [PubMed: 27281221]
12. Narayanam MK, Ma G, Champagne PA, Houk KN,Murphy JM, Angew. Chem. Int. Ed 56, 13006–13010 (2017).
13. Gendron T et al., J. Am. Chem. Soc 140, 11125–11132 (2018). [PubMed: 30132661]
14. Lee E et al., Science 334, 639–642 (2011). [PubMed: 22053044]
15. Lee E, Hooker JM, Ritter T, J. Am. Chem. Soc 134, 17456–17458 (2012). [PubMed: 23061667]
16. Ichiishi N et al., Org. Lett 16, 3224–3227 (2014). [PubMed: 24890658]
17. McCammant MS et al., Org. Lett 19, 3939–3942 (2017). [PubMed: 28665619]
18. Mossine AV et al., Org. Lett 17, 5780–5783 (2015). [PubMed: 26568457]
19. Tredwell M et al., Angew. Chem. Int. Ed 53, 7751–7755 (2014).
20. Makaravage KJ, Brooks AF, Mossine AV, Sanford MS,Scott PJH, Org. Lett 18, 5440–5443 (2016). [PubMed: 27718581]
21. Sasson Y et al., ACS Symp. Ser 659, 148–162 (1997).
22. Harper KC, Moschetta EG, Bordawekar SV,Wittenberger SJ, ACS Cent. Sci 5, 109–115 (2019). [PubMed: 30693330]
23. Romero NA, Margrey KA, Tay NE, Nicewicz DA, Science 349, 1326–1330 (2015). [PubMed: 26383949]
24. McManus JB, Nicewicz DA, J. Am. Chem. Soc 139, 2880–2883 (2017). [PubMed: 28177237]
25. Margrey KA, McManus JB, Bonazzi S, Zecri F,Nicewicz DA, J. Am. Chem. Soc 139, 11288–11299 (2017). [PubMed: 28718642]
26. Vitaku E, Smith DT, Njardarson JT, J. Med. Chem 57, 10257–10274 (2014). [PubMed: 25255204]
27. Laube M, Kniess T, Pietzsch J, Molecules 18, 6311–6355 (2013). [PubMed: 23760031]
28. Deng X et al., Angew. Chem. Int. Ed 58, 2580–2605 (2019).
29. Park BK, Kitteringham NR, O'Neill PM, Annu. Rev. Pharmacol. Toxicol 41, 443–470 (2001). [PubMed: 11264465]
30. Koerts J, Soffers AEMF, Vervoort J, De Jager A,Rietjens IMCM, Chem. Res. Toxicol 11, 503–512 (1998). [PubMed: 9585481]
31. Shah P, Westwell AD, Enzyme Inhib J. Med. Chem 22, 527–540 (2007).
32. Penning TD et al., J. Med. Chem 40, 1347–1365 (1997). [PubMed: 9135032]
33. Lebedev A et al., PLOS ONE 12, e0176606 (2017). [PubMed: 28464017]
34. Cryer B, Feldman M, Am. J. Med 104, 413–421 (1998). [PubMed: 9626023]
35. Isin EM, Elmore CS, Nilsson GN, Thompson RA,Weidolf L, Chem. Res. Toxicol 25, 532–542 (2012). [PubMed: 22372867]

36. Pretze M et al., Nucl. Med. Biol 45, 35–42 (2017). [PubMed: 27886621]
37. Pretze M, Wängler C, Wängler B, BioMed Res. Int 2014, 674063 (2014). [PubMed: 24987698]
38. Brogden RN, Finder RM, Speight TM, Avery GS, Drugs 13, 241–265 (1977). [PubMed: 324748]
39. Madsen M et al., BMC Dermatol. 16, 9 (2016). [PubMed: 27401543]
40. Zhu A, Shim H, Nucl. Med. Mol. Imaging 45, 1–14 (2011). [PubMed: 24899972]
41. Qi Y, Liu X, Li J, Yao H, Yuan S, Oncotarget 8, 60581–60588 (2017). [PubMed: 28947996]
42. Sun A, Liu X, Tang G, Front Chem. 5, 124 (2018). [PubMed: 29379780]
43. Chen W, Huang Z, Tay N, Giglio B, Wang M, Wang H, Wu Z,Nicewicz D, Li Z, #39 in MCF-7 and U87MG tumor models at different time points, Zenodo (2019); 10.5281/zenodo.3228508.
44. Chen W, Huang Z, Tay N, Giglio B, Wang M, Wang H, Wu Z,Nicewicz D, Li Z, #41 in MCF-7 tumor model at different time points, Zenodo (2019); 10.5281/zenodo.3228551.
45. Chen W, Huang Z, Tay N, Giglio B, Wang M, Wang H, Wu Z,Nicewicz D, Li Z, #42 in ear inflammation model, Zenodo (2019); 10.5281/zenodo.3228546.
46. Chen W, Huang Z, Tay N, Giglio B, Wang M, Wang H, Wu Z,Nicewicz D, Li Z, #42 dynamic PET scan, Zenodo (2019); 10.5281/zenodo.3228534.
47. Chen W, Huang Z, Tay N, Giglio B, Wang M, Wang H, Wu Z,Nicewicz D, Li Z, File index, Zenodo (2019); 10.5281/zenodo.3228554.

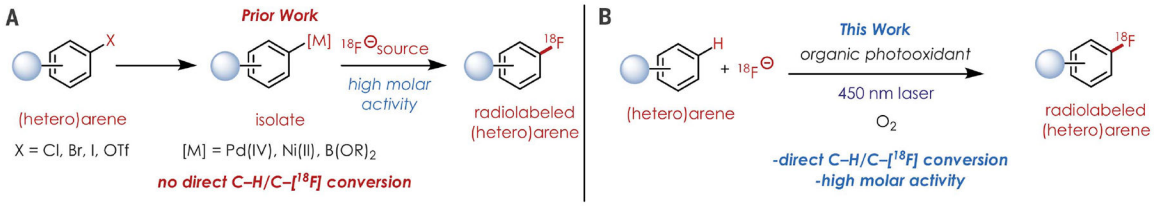

Fig. 1. An organic photoredox approach to ^{18}F labeling of arenes for PET studies.

(A) Prior work relies on the isolation of aryl organometallic species. (**B**) This study obviates the need for metalation by using organic photoredox catalysis.

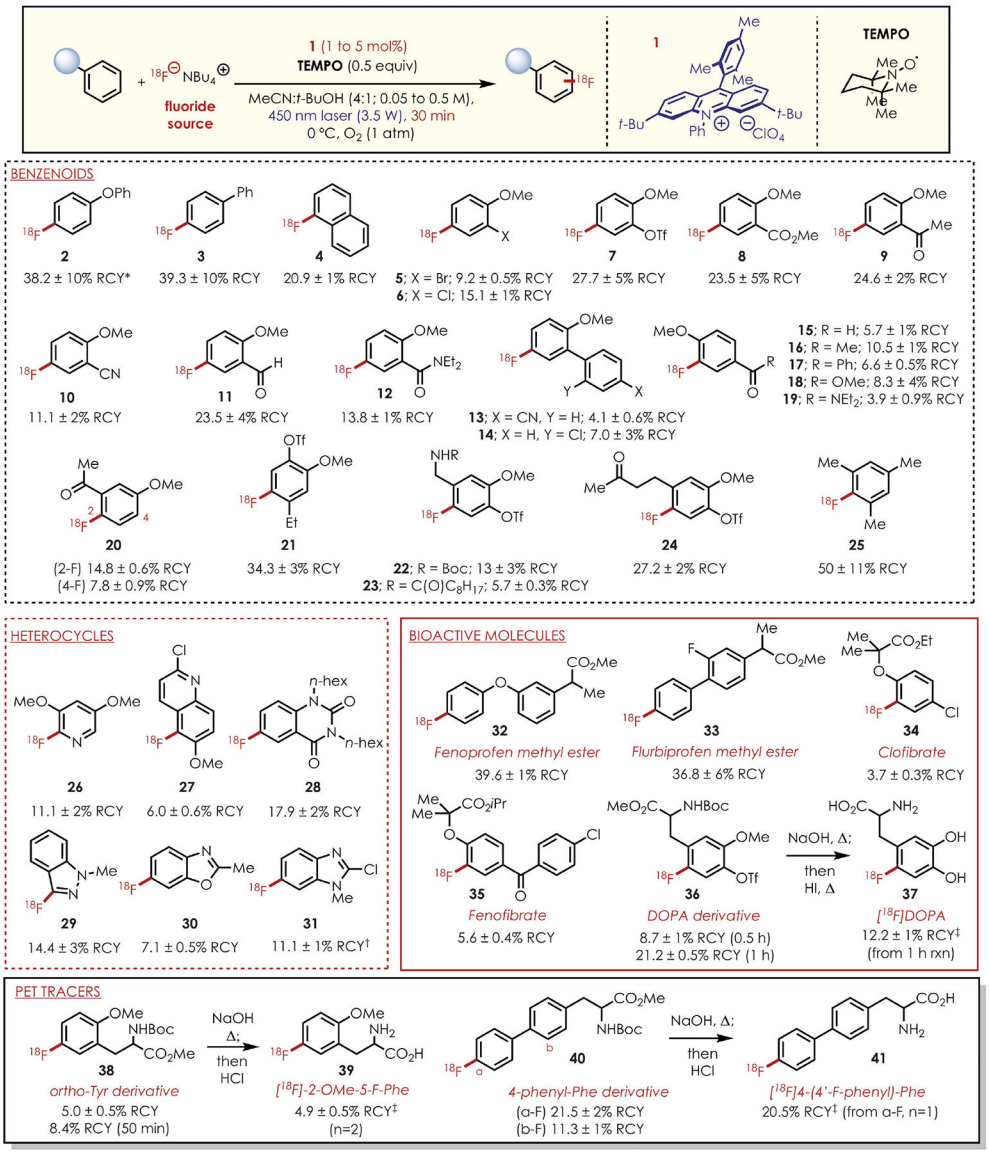

Fig. 2. Reaction scope of ^{18}F-fluorination of aromatics.

All RCYs are decay-corrected and averaged over three experiments unless otherwise noted. Asterisk indicates yield averaged over five experiments. Single-dagger symbol indicates that 24.8% RCY of the 2-fluoro dechlorinated product is formed. Double-dagger symbol indicates that the RCYs listed are based on the product deprotection yields (see SM 5.6). Bu, butyl; MeCN, acetonitrile; hex, hexyl; iPr, isopropyl; t-Bu, tert-butyl; Me, methyl; Ph, phenyl; OTf, trifluoromethanesulfonate; Et, ethyl; Boc, butoxycarbonyl.

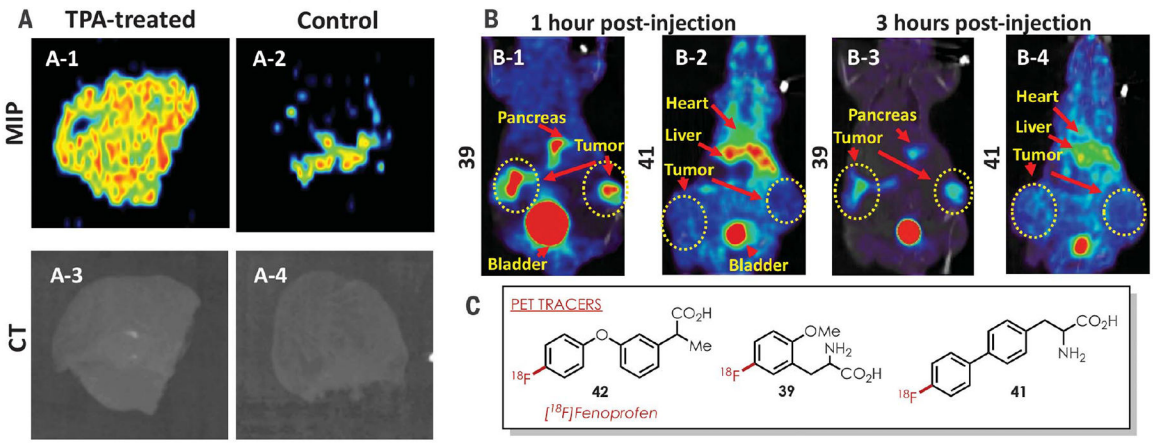

Fig. 3. Examples of PET tracers synthesized via arene C–H radiofluorination.

(A) Maximum intensity projection (MIP) PET images of [^{18}F]-fenoprofen (**42**) demonstrate higher uptake in TPA-treated mouse ear (A-1) compared with control (A-2) mouse ear. (**B**) PET/CT images demonstrate preferential tumor (MCF-7) accumulation of **39**, compared with longer blood circulation and higher nonspecific binding of **41** at 1 hour after injection. (**C**) Structures of the tracers used in the preceding panels are shown.